Supporting Information

Surface decoration of Ba-enriched Fe-based air electrodes with Co-based catalysts for robust protonic ceramic electrochemical cells

Yan Liu,[a,†] Haoqing Lin,[a,†] Jingnan Zou,[a] Tenghui Yuan,[a] Zhuohao Wang,[a] Hang Bao,[a] Ali Abdelhafiz,[c] and Bote Zhao[*a,b]

[a] School of Environment and Energy, South China University of Technology, Guangzhou 510006, China.

[b] Guangdong Provincial Key Laboratory of Atmospheric Environment and Pollution Control, Guangzhou 510006, China.

[c] Department of Nuclear Science and Engineering, Massachusetts Institute of Technology, 77 Mass Ave, Cambridge, MA 02139, USA.

[*]Corresponding author:

Bote Zhao, E-mail: botezhao@scut.edu.cn

[†] These authors contributed equally to this work.

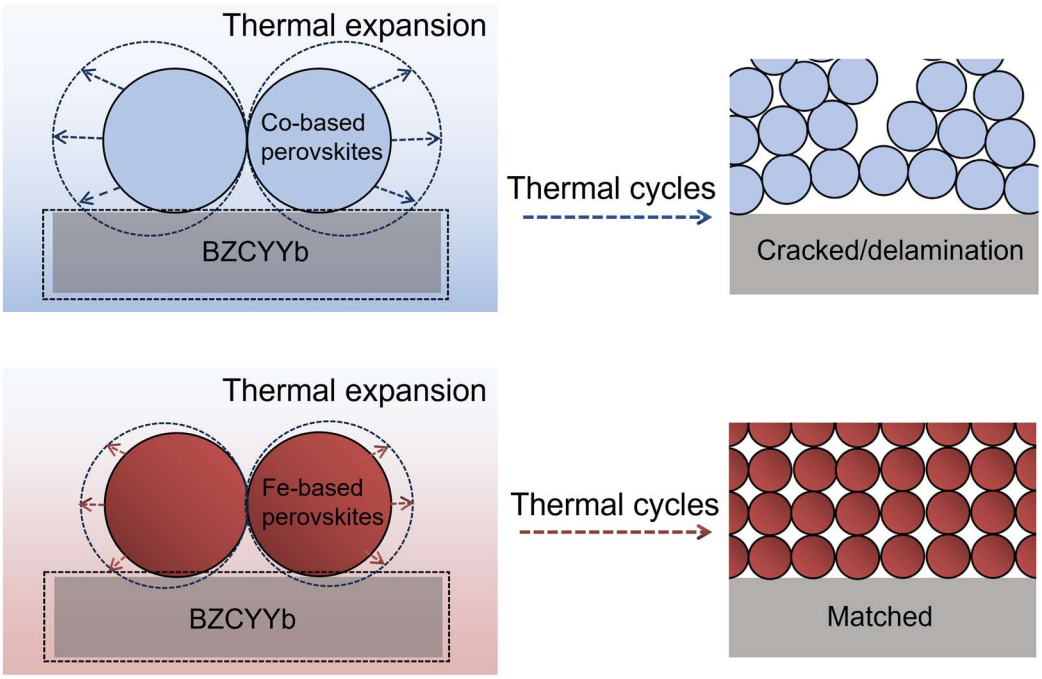

Figure S1. Schematic illustration of potential thermal expansion mismatch issues in PCECs.

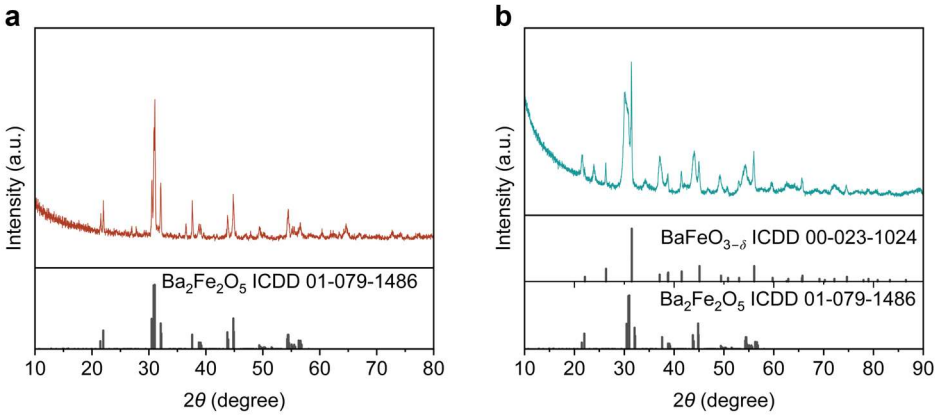

Figure S2. XRD patterns of **(a)** BF and **(b)** $B_{1.02}F$ powders.

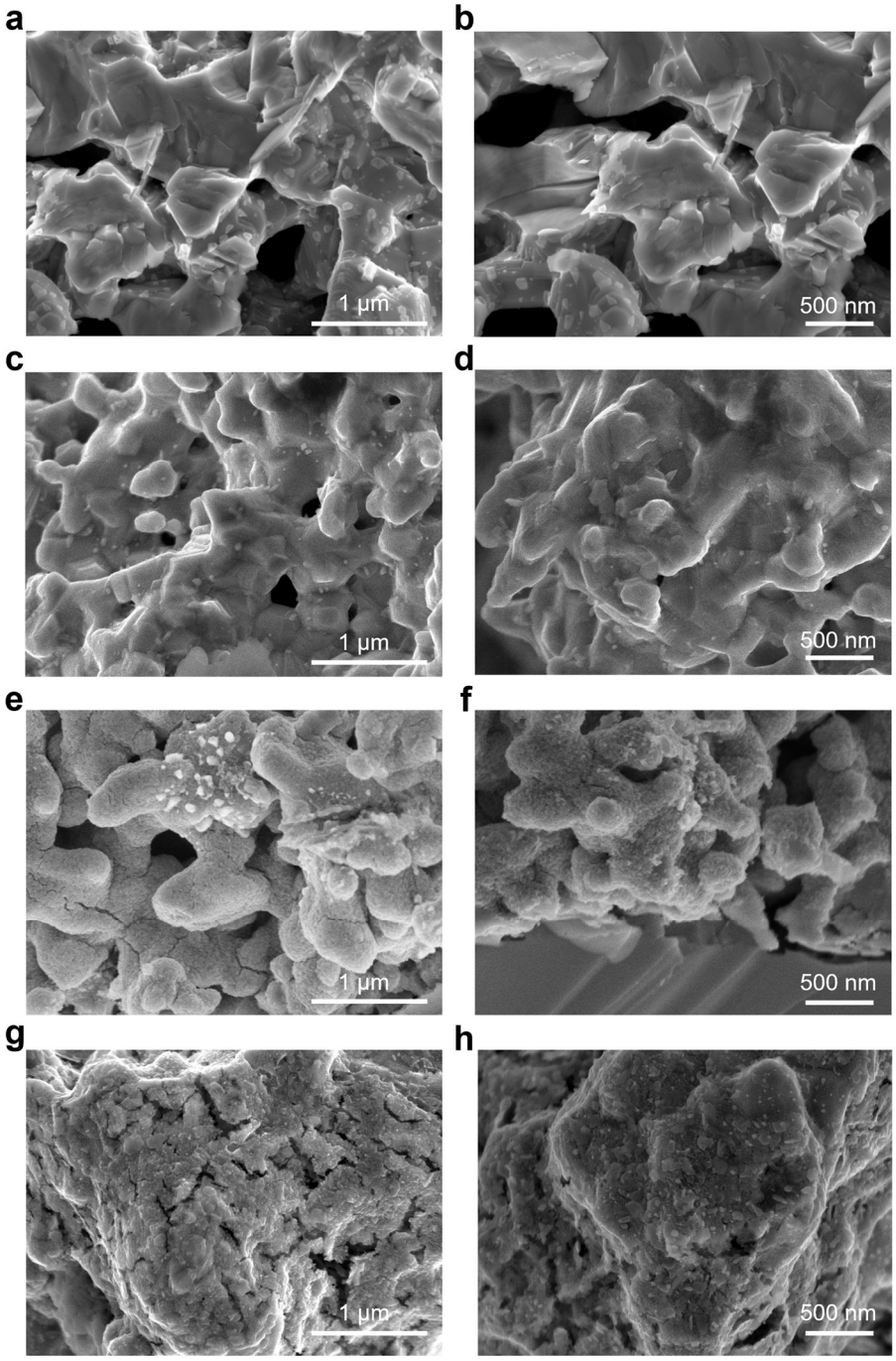

Figure S3. SEM images of the air electrodes. **(a, b)** bare BF; and **(c-h)** $B_{1.02}F$-CC prepared with different infiltration volumes of 0.1 M $Co(NO_3)_2$ precursor solution: **(c, d)** 2 μL, **(e, f)** 4 μL, and **(g, h)** 6 μL. The 2, 4, and 6 μL volumes correspond to equivalent Co_3O_4 catalyst loadings of 1.8, 3.6, and 5.4 wt.%, respectively.

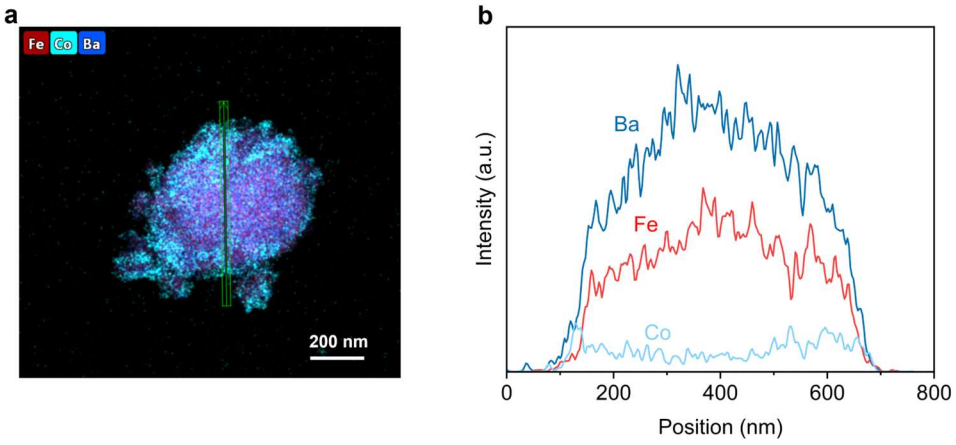

Figure S4. (a) EDS elemental mapping of $B_{1.02}F$-CC; **(b)** corresponding EDS line-scan profile along the line marked in **(a)**.

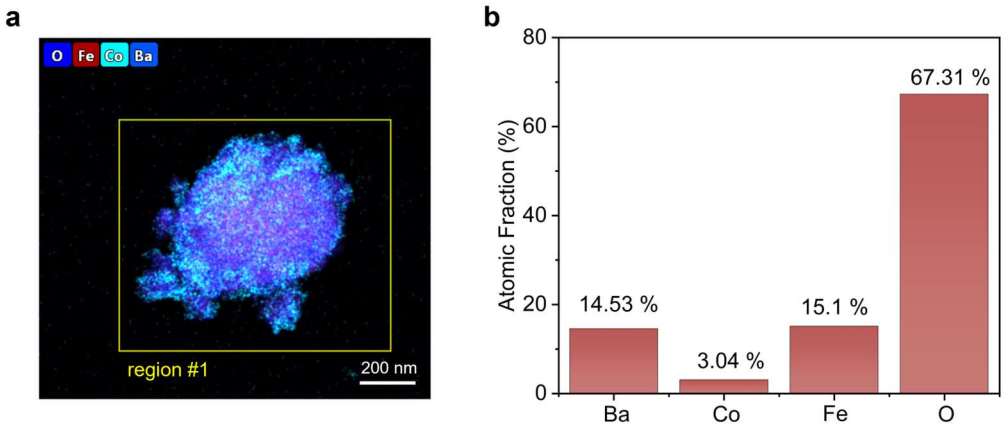

Figure S5. (a) EDS elemental mapping of $B_{1.02}F$-CC; **(b)** atomic fractions of the region marked as region #1.

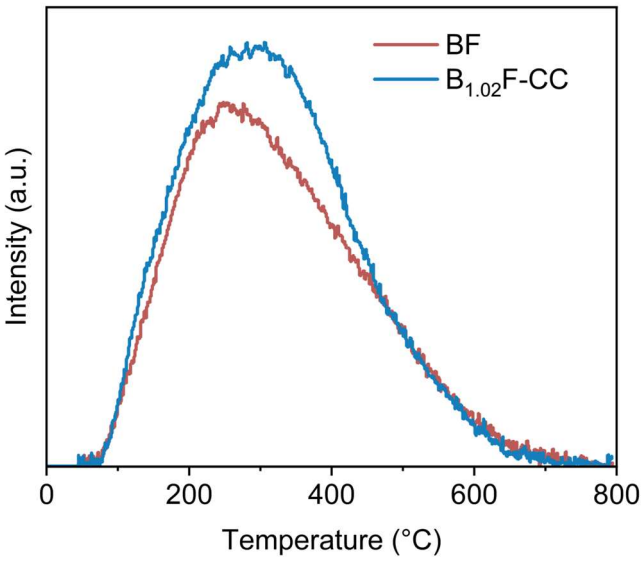

Figure S6. H_2O-TPD profiles of BF and $B_{1.02}F$-CC samples from 50 °C to 800 °C.

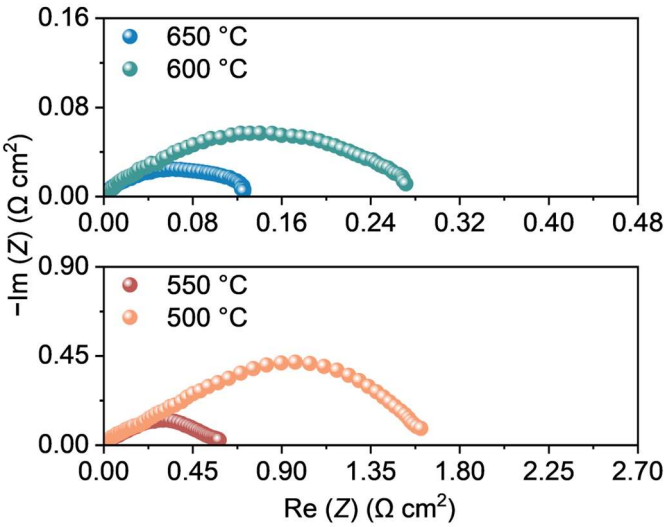

Figure S7. Nyquist plots of the symmetric cell with $B_{1.02}F$ air electrode measured at different temperatures.

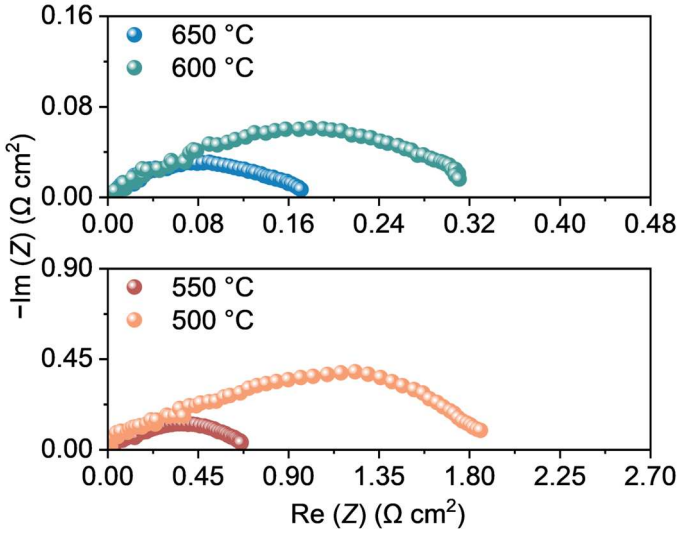

Figure S8. Nyquist plots of the symmetric cell with $B_{1.02}F$-1000 air electrode measured at different temperatures.

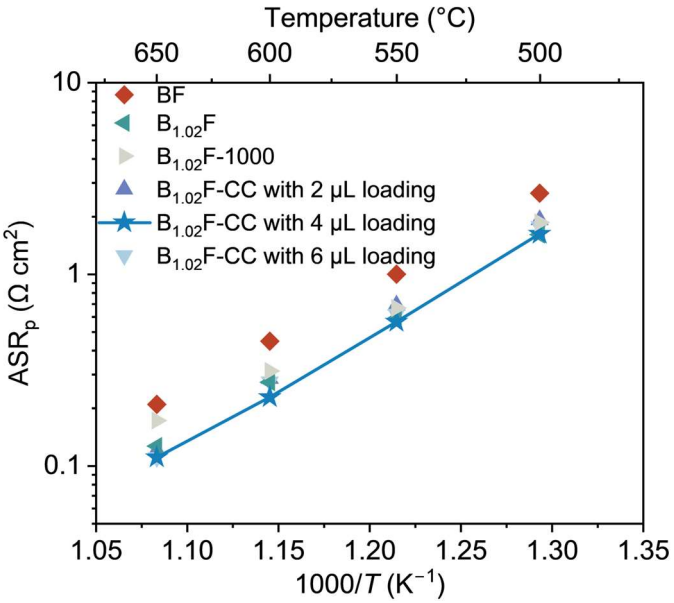

Figure S9. Arrhenius-type plots of ASR_p for BF, $B_{1.02}F$, $B_{1.02}F$-1000, and $B_{1.02}F$-CC air electrodes prepared with different volumes of 0.1 M $Co(NO_3)_2$ precursor solution. These infiltration volumes of 2, 4, and 6 μL correspond to equivalent Co_3O_4 mass fractions of approximately 1.8, 3.6, and 5.4 wt.%, respectively.

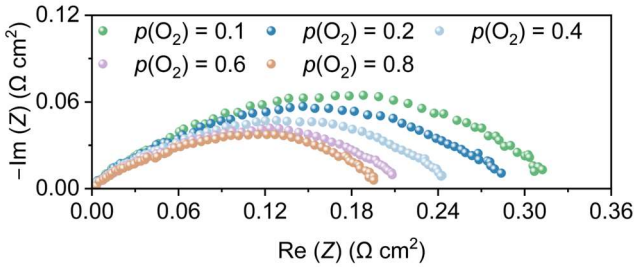

Figure S10. Nyquist plots of symmetric cells employing $B_{1.02}F$-CC air electrodes, recorded at 600 °C in wet air (3% H_2O) under different $p(O_2)$.

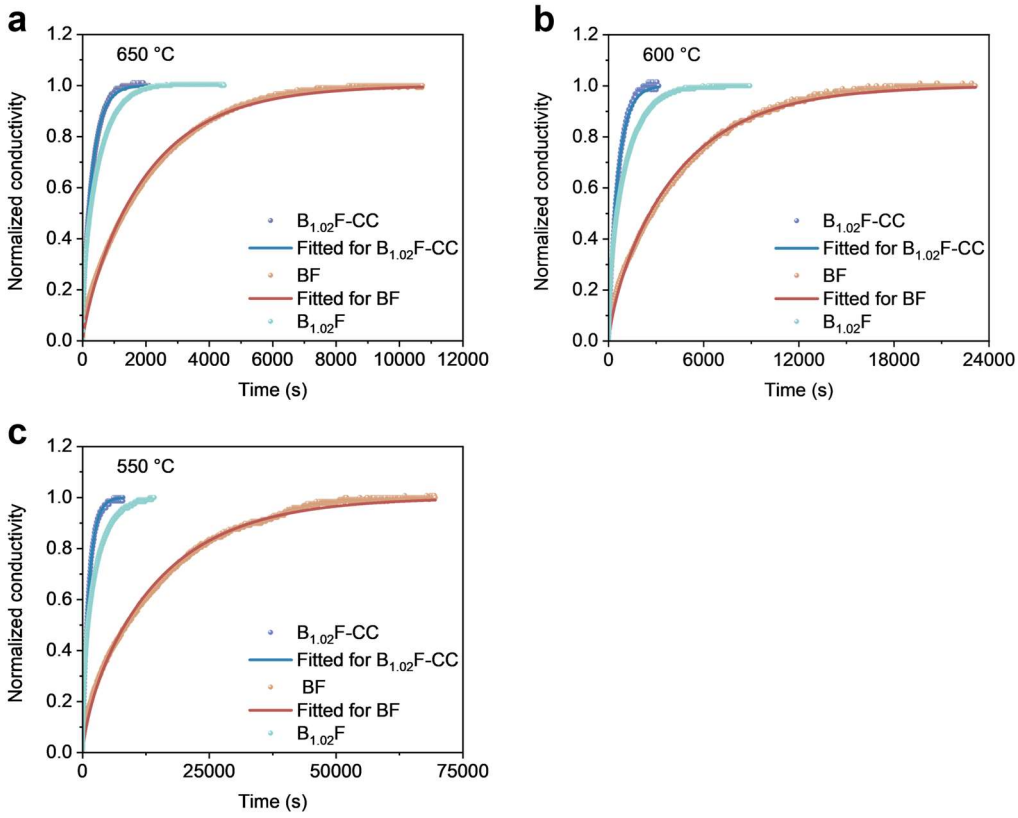

Figure S11. ECR curves of $B_{1.02}$F-CC, $B_{1.02}$F, and BF recorded at **(a)** 650 °C, **(b)** 600 °C, and **(c)** 550 °C.

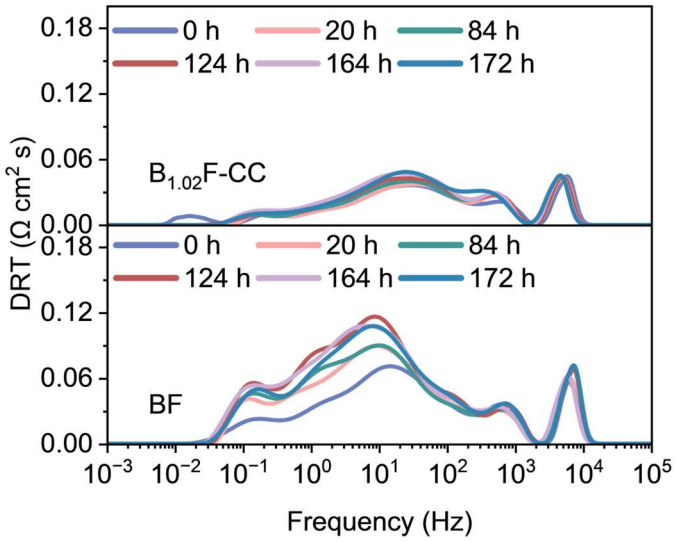

Figure S12. DRT analysis of $B_{1.02}$F-CC and BF air electrodes at various points throughout the durability test.

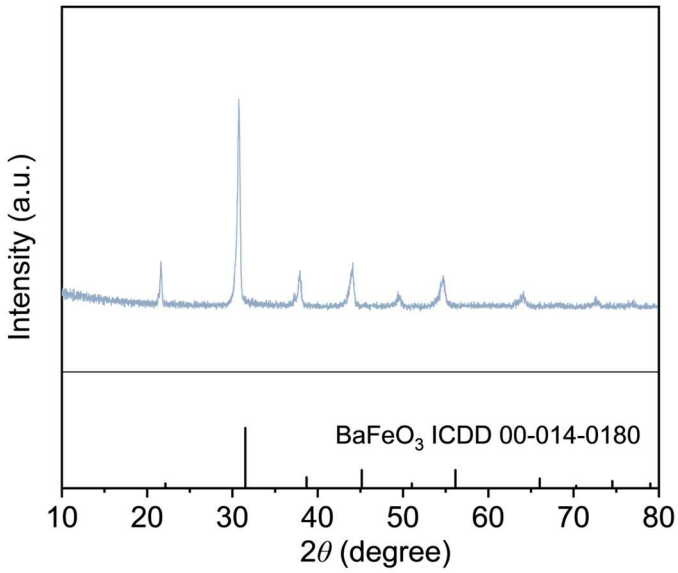

Figure S13. XRD pattern of BCF powder.

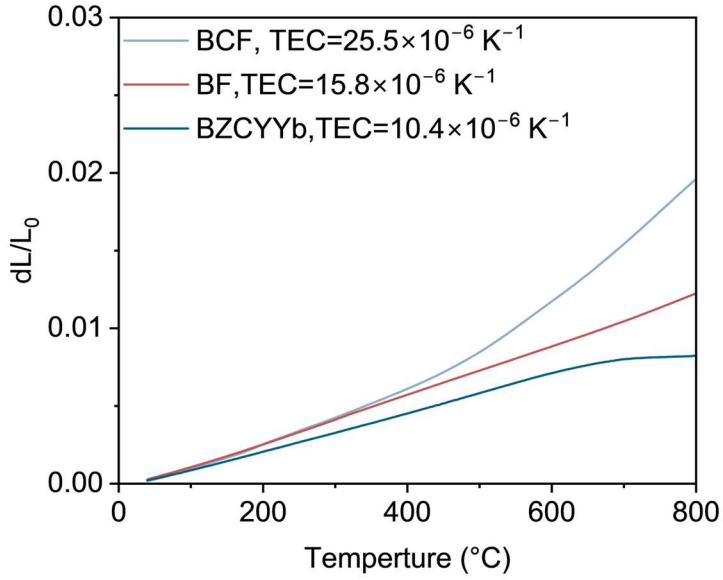

Figure S14. Thermal expansion curves of dense BZCYYb, BF, and BCF bars measured in air from room temperature to 800 °C.

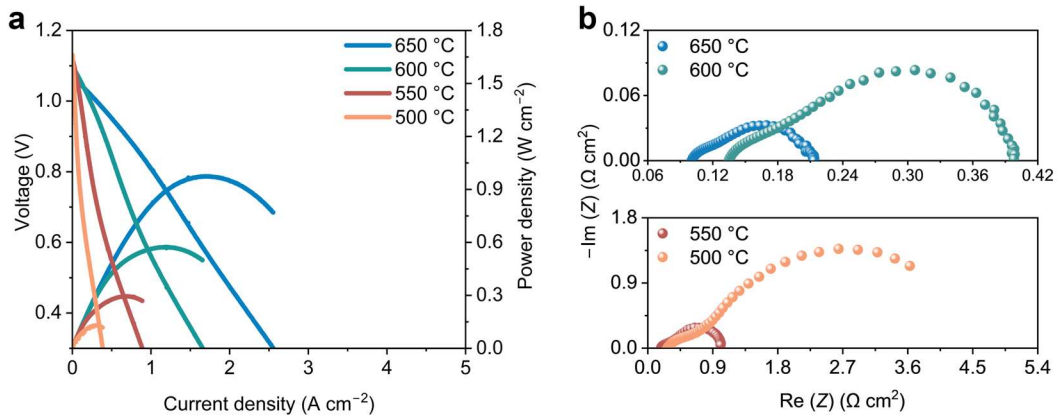

Figure S15. Fuel-cell mode performance of the single cell with the BF air electrode at different temperatures. (a) *I-V-P* curves; **(b)** Nyquist plots measured under OCV conditions.

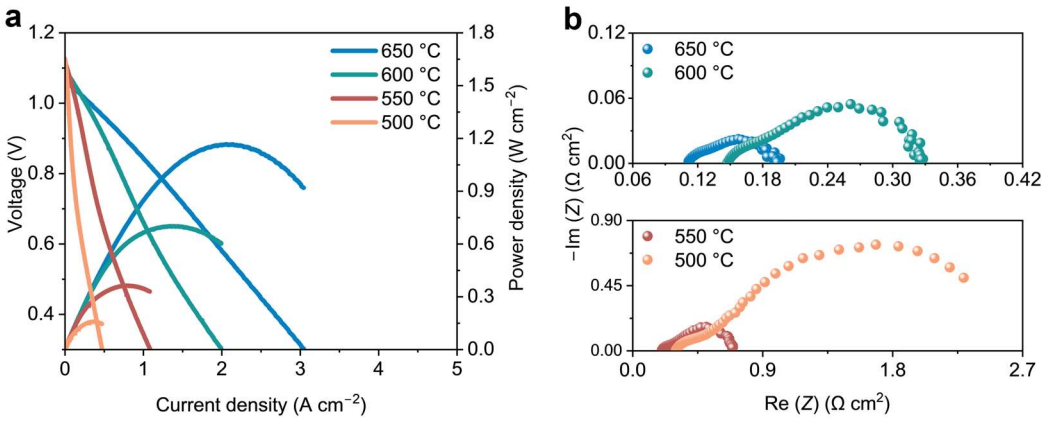

Figure S16. Fuel-cell mode performance of the single cell with the $B_{1.02}F$ air electrode at different temperatures. (a) *I-V-P* curves; **(b)** Nyquist plots measured under OCV conditions.

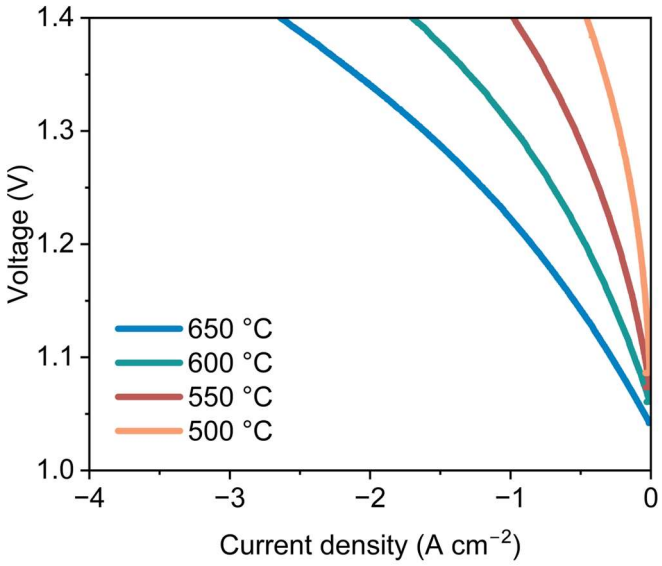

Figure S17. Electrolysis performance of the single cell utilizing the BF air electrode.

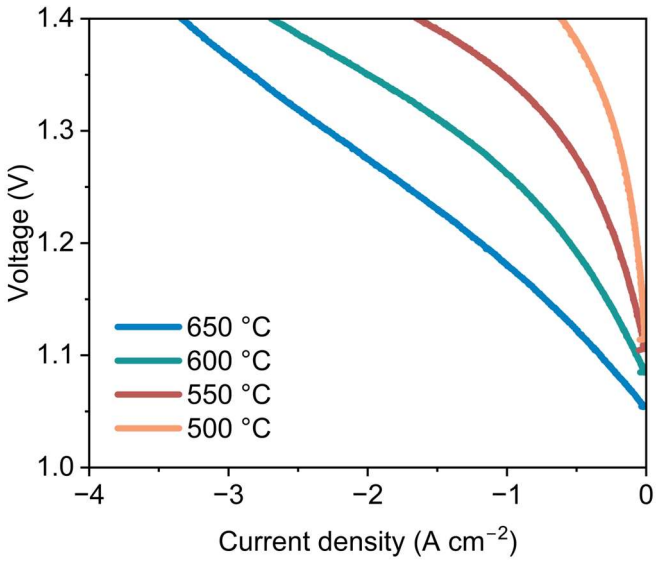

Figure S18. Electrolysis performance of the single cell utilizing the $B_{1.02}F$ air electrode.

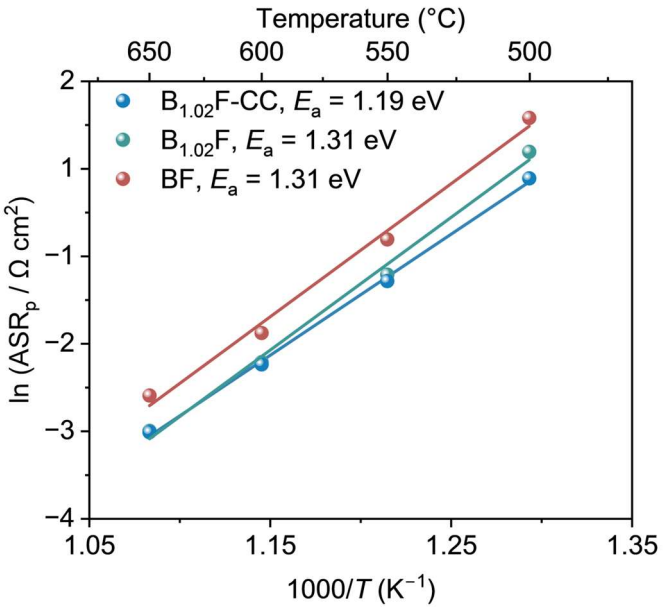

Figure S19. Arrhenius-type plots of ASR_p for the single cell utilizing BF, $B_{1.02}F$, and $B_{1.02}F$-CC air electrodes.

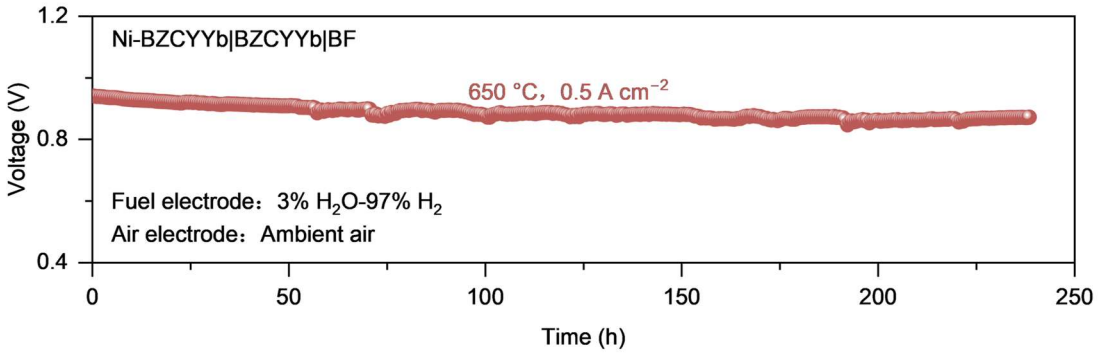

Figure S20. Long-term stability test of the single cell utilizing BF air electrode at 650 °C under a constant current density of 0.5 A cm^{-2}.

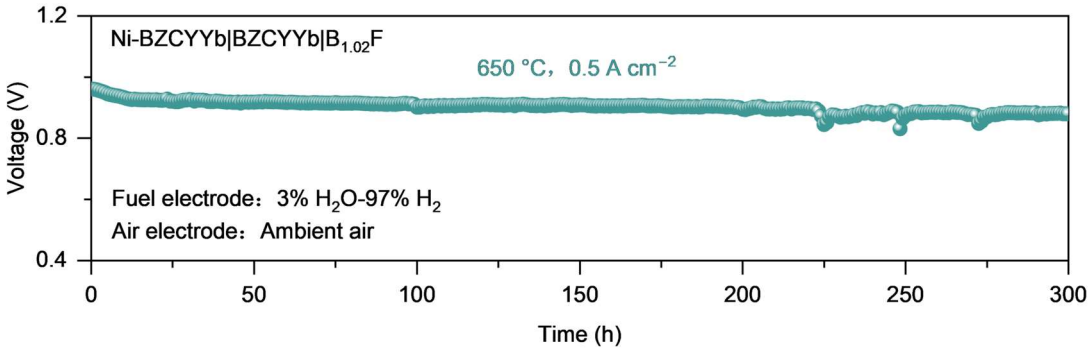

Figure S21. Long-term stability test of the single cell utilizing $B_{1.02}F$ air electrode at 650 °C under a constant current density of 0.5 A cm^{-2}.

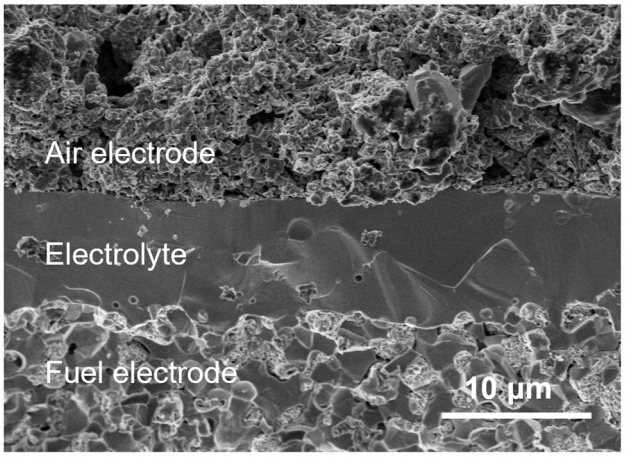

Figure S22. Cross-sectional SEM image of the single cell with the $B_{1.02}F$-CC air electrode after long-term stability test for 600 h at 650 °C in fuel-cell mode.

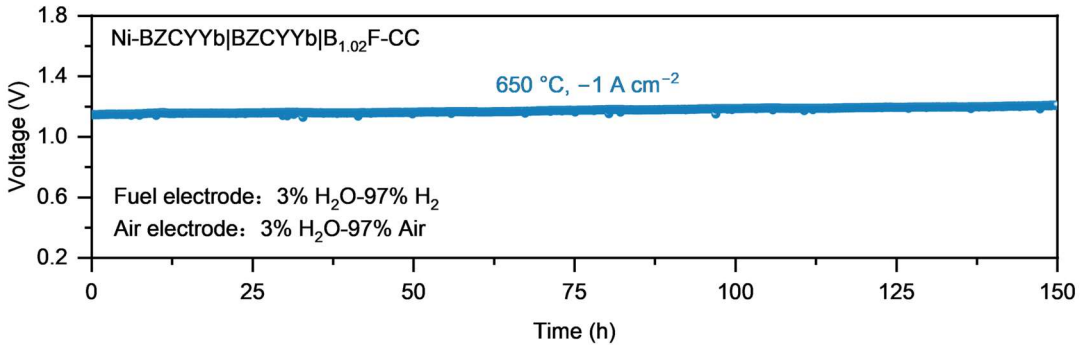

Figure S23. Long-term stability test of the single cell utilizing $B_{1.02}F$-CC air electrode at 650 °C under a constant current density of −1 A cm^{-2} in electrolysis mode.

Table S1. Summary of ASR_p values for $B_{1.02}F$-CC and other advanced air electrodes measured in symmetric cells.

Air electrode	ASR_p (Ω cm^2)				Ref.
	650 °C	600 °C	550 °C	500 °C	
$B_{1.02}F$-CC	0.110	0.227	0.562	1.62	This wok
PBSCaC ($Pr_{0.5}Ba_{1/6}Sr_{1/6}Ca_{1/6}CoO_{3-\delta}$)	0.155	0.348	0.842	2.298	*Energy Environ. Sci*., **2024**, 17, 7782-7791[49]
PNC-LSCF ($Pr_2Ni_{0.5}Co_{0.5}O_{4-\delta}$-$La_{0.6}Sr_{0.4}Co_{0.2}Fe_{0.8}O_{3-\delta}$)	0.167	0.42	1.46	N.A.[a]	*Adv. Energy Mater*., **2025**, 15, 2403335[51]
HE-PBSLCaC (High-entropy $Pr_{0.2}Ba_{0.2}Sr_{0.2}La_{0.2}Ca_{0.2}CoO_{3-\delta}$)	0.12	0.26	0.75	2.13	*Adv. Mater*., **2023**, 35, 2209469[46]
MCsCO-CO ($Mn_{0.9}Cs_{0.1}Co_2O_{4-\delta}$-$Co_3O_4$)	0.176	0.382	0.984	2.94	*Adv. Mater*., **2024**, 36, 2408044[50]
CePLBSCaC ($Ce_{0.05}Pr_{0.19}La_{0.19}Ba_{0.19}Sr_{0.19}Ca_{0.19}CoO_{3-\delta}$)	0.13	0.29	0.71	1.99	*Adv. Funct. Mater*., **2025**, e25122[48]
PBCsC ($PrBa_{0.9}Cs_{0.1}Co_2O_{5+\delta}$)	0.162	0.275	0.531	1.526	*ACS Energy Lett*., **2023**, 8, 4145-4155[47]

[a] N.A. = Not available

Table S2. Summary of fuel-cell mode performance for the $B_{1.02}F$-CC and other high-performance air electrodes reported recently.

Air electrode	P_{max} (W cm^{-2})				Ref.
	650 °C	600 °C	550 °C	500 °C	
$B_{1.02}F$-CC	1.46	1.06	0.68	0.38	This work
BCeFNb ($BaCe_{0.1}Fe_{0.8}Nb_{0.1}O_{3-\delta}$)	1.091	0.82	0.559	0.324	*Adv. Funct. Mater*., **2025**, 35, 2502771[62]
BSCsCFZ ($Ba_{0.4}Sr_{0.5}Cs_{0.1}Co_{0.7}Fe_{0.2}Zr_{0.1}O_{3-\delta}$)	1.240	0.936	0.638	0.338	*Adv. Funct. Mater*., **2025**, 35, 2422531[57]
BSCFEr ($Ba_{0.5}Sr_{0.5}(Co_{0.8}Fe_{0.2})_{0.9}Er_{0.1}O_{3-\delta}$)	1.327	0.984	0.701	0.525	*Adv. Funct. Mater*., **2024**, 34, 2311140[60]
MCsCO-CO ($Mn_{0.9}Cs_{0.1}Co_2O_{4-\delta}$-$Co_3O_4$)	1.34	0.97	0.62	0.28	*Adv. Mater*., **2024**, 36, 2408044[50]
NiO-XFN (*x*NiO-$Pr_{0.2}La_{0.2}Ba_{0.2}Sr_{0.2}Ca_{0.2}Fe_{0.8}Ni_{0.2-x}O_{3-\delta}$)	1.30	0.79	0.43	N.A.[a]	*Adv. Energy Mater*., **2025**, 15, 2405466[41]
PNC-LSCF ($Pr_2Ni_{0.5}Co_{0.5}O_{4-\delta}$-$La_{0.6}Sr_{0.4}Co_{0.2}Fe_{0.8}O_{3-\delta}$)	1.291	1.023	0.662	N.A.	*Adv. Energy Mater*., **2025**, 15, 2403335[51]
BSCFW@PBSCF ((Ba/Sr)(Co/Fe/W)$O_{3-\delta}$)@$PrBa_{0.5}Sr_{0.5}Co_{1.5}Fe_{0.5}O_{5+\delta}$)	1.32	0.90	0.57	N.A.	*Adv. Mater.*, **2024**, 36, 2405052[61]
BGCO ($Ba_{1+x}Gd_{1-x}Co_2O_{6-\delta}$)	0.872	0.604	0.386	0.189	*Adv. Energy Mater*., **2024**, 14, 2400319[59]
SCNb-PSCNb ($SrCo_{0.5}Nb_{0.5}O_{3-\delta}$-$PrSrCo_{1.8}Nb_{0.2}O_{6-\delta}$)	1.30	0.94	0.60	N.A.	*ACS Nano*, **2024**, 18, 5141-5151[58]
2Ru-BCeF ($BaCe_{0.125}Fe_{0.875}O_{3-\delta}$ with 2 wt.% Ru)	1.38	0.97	0.58	N.A.	*Adv. Mater*., **2025**, 37, 2501387[26]

[a] N.A. = Not available

Table S3. Summary of electrolysis mode performance for the $B_{1.02}F$-CC and other high-performance air electrodes reported recently.

Air electrode	Current densities at 1.3 V(A cm^{-2})				Ref.
	650 °C	600 °C	550 °C	500 °C	
$B_{1.02}F$-CC	−2.81	−1.72	−0.90	−0.40	This work
SFMo-0.05SnO_2 ($Sr_2Fe_{1.5}Mo_{0.5}O_{6-\delta}-0.05SnO_2$)	−2.09	−1.40	−0.57	−0.25	*Adv. Funct. Mater*., **2025**, 36, e17821[66]
NiO-XFN (*x*NiO-$Pr_{0.2}La_{0.2}Ba_{0.2}Sr_{0.2}Ca_{0.2}Fe_{0.8}Ni_{0.2-x}O_{3-\delta}$)	−2.52	−1.70	−0.92	N.A.[a]	*Adv. Energy Mater*., **2025**, 15, 2405466[41]
BCFZYCe-CeO_2 (Ce-doped $BaCo_{0.4}Fe_{0.4}Zr_{0.1}Y_{0.1}O_{3-\delta}$ with exsolved CeO_2)	−1.47	−1.16	−0.73	−0.42	*Adv. Funct. Mater*., **2025**, 36, e16197[64]
MCsCO-CO ($Mn_{0.9}Cs_{0.1}Co_2O_{4-\delta}$-$Co_3O_4$)	−2.48	−1.45	−0.56	−0.24	*Adv. Mater*., **2024**, 36, 2408044[50]
BSCsCFZ ($Ba_{0.4}Sr_{0.5}Cs_{0.1}Co_{0.7}Fe_{0.2}Zr_{0.1}O_{3-\delta}$)	−1.98	−1.23	−0.787	N.A.	*Adv. Funct. Mater*., **2025**, 35, 2422531[57]
HE-PBSLCaC (High-entropy $Pr_{0.2}Ba_{0.2}Sr_{0.2}La_{0.2}Ca_{0.2}CoO_{3-\delta}$)	−2.68	−1.75	−0.80	−0.28	*Adv. Mater*., **2023**, 35, 2209469[46]
bs-PBSCF (Ba/Sr-deficient $Pr(Ba_{0.5}Sr_{0.5})_{0.95}Co_{1.5}Fe_{0.5}O_{5+\delta}$)	N.A.	−1.28	−0.822	−0.511	*Adv. Mater*., **2025**, 37, e11519[65]
CCS-PBN (Conformally coated scaffold-$Pr_{1.8}Ba_{0.2}NiO_{4.1}$)	−2.4	−1.46	−0.68	N.A.	*Nat. Energy*, **2025**, 10, 890-903[29]
PBSCN20 ($PrBa_{0.5}Sr_{0.5}Co_{1.8}Ni_{0.2}O_{5+\delta}$)	N.A.	−1.72	N.A.	−0.41	*Adv. Funct. Mater*., **2025**, 35, 2508758[63]
BSCFEr ($Ba_{0.5}Sr_{0.5}(Co_{0.8}Fe_{0.2})_{0.9}Er_{0.1}O_{3-\delta}$)	−2.23	−1.54	−1.05	−0.56	*Adv. Funct. Mater*., **2024**, 34, 2311140[60]

[a] N.A. = Not available